PHYSICAL REVIEW B **69**, 155306 (2004)

Nanoindentation and near-field spectroscopy of single semiconductor quantum dots

A. M. Mintairov, K. Sun, and J. L. Merz
Electrical Engineering Department, University of Notre Dame, Notre Dame, Indiana 46556, USA

C. Li
Aerospace and Mechanical Engineering Department, University of Notre Dame, Notre Dame, Indiana 46556, USA

A. S. Vlasov, D. A. Vinokurov, and O. V. Kovalenkov
A. F. Ioffe Physical-Technical Institute, RAS, 26 Polytechnicheskaya, St. Petersburg, Russia 194021

V. Tokranov and S. Oktyabrsky
Institute for Materials, State University of New York at Albany, 251 Fuller Road, Albany, New York 12203, USA

(Received 6 June 2003; revised manuscript received 23 September 2003; published 5 April 2004)

Low-temperature near-field scanning optical microscopy was used to study the dependence of the emission spectra of single self-organized InAs on GaAs, InAs on AlAs and InP on GaInP quantum dots (QDs) on contact pressure exerted by a near-field optical fiber tip (nanoindentation). A large energy shift (up to 150 meV), broadening (up to 10 meV), and intensity increase (up to one order of magnitude) of single QD emission lines have been observed at tip compressions up to 70 nm. Ground state energy shift rates from 0.5 to 3.5 meV/nm have been measured for different aperture types (rounded and flat, metal coated and uncoated) and sizes (50–300 nm) in agreement with numerical calculations using Picus–Bir orbital-strain Hamiltonian. A reduction of the hydrostatic pressure coefficient due to a nonuniform In distribution in self-organized QDs has been observed. Anomalously strong lateral inhomogeneity of the local stress field has been observed.

DOI: 10.1103/PhysRevB.69.155306 PACS number(s): 73.21.−b, 78.66.Fd, 78.55.Cr

I. INTRODUCTION

The coupling of the evanescent electromagnetic field and the radiative electromagnetic waves in the vicinity of a nanoprobe placed near the boundary between two media is a basic principle of near-field optics, providing a way to overcome the diffraction limit of light of conventional optics.[1] The realization of this principle nearly two decades ago using nanoapertures,[2,3] metallic,[4] and dielectric[5,6] nanotips gives rise to the development of the near-field optical scanning microscope (NSOM),[7–10] allowing nanometer-scale spatial resolution in optical experiments. Among the many different and unique applications of NSOM (Refs. 11–16) is the possibility of optical spectroscopic experiments with single semiconductor quantum dots (QDs).[17–32] The novel atomic-like electronic properties of semiconductor QDs arising from strong mesoscopic heterointerface potentials and the ability to control their properties using strained layer epitaxial growth present very attractive opportunities for investigating the physics of quantum structures,[33] photonics and electronics application,[34] and the demonstration of quantum computing processing.[35–37] High spatial resolution and the nondestructive character of the experiment, in combination with high magnetic field and time resolved techniques[20,23,38] allows the use of NSOM to study structural parameters,[22,27] spin fine structure of exciton states,[21,39] temporal coherence of wave functions,[25] and mechanisms of carrier migration[40] and relaxation[41] in QDs.

The NSOM technique may also be used to produce highly localized stress to the sample through the nanoprobe, exactly as is done in nanoindentation experiments to study material hardness.[42] This can extend the methods of the piezo-spectroscopy[43–45] to the nanoscale region, allowing piezo-spectroscopy of a single QD to be realized. However little is known about the effect of tip-induced stress on QD energy levels and about indentation properties of NSOM nanoprobes. There are only a few reports of NSOM spectroscopic study of single QDs in the nanoindentation regime.[46–49] These reports demonstrated an increase of the emission energy of the QDs under loading conditions but only for a limited number of indentation points. No detailed analysis of the stress produced by the NSOM tip is presented in the literature.

In the present paper we used low-temperature near-field photoluminescence spectroscopy to study emission properties of single self-organized QDs under nanoindentation using an optical fiber probe for a variety of structures (InAs/AlAs, InAs/GaAs, and InP/GaInP), probe types (rounded and flat, metal coated and uncoated) and sizes (50–300 nm). Finite element analysis of the stress distribution and of the ground state energy shift of QDs have been performed. Near-field magnetophotoluminescence measurements of the diamagnetic shift were used to distinguish dots of different sizes, In content, and homogeneity. This allows a correlation of specific structural properties of the QDs, arising from bimodal size distribution, with their optical properties: emission energy and spectral dependence on local stress. High energy shifts (up to 150 meV), broadening (up to 10 meV), and intensity increase (up to one order of magnitude) of the emission from single QDs have been observed at tip compressions 30–70 nm. ‘‘Pressure’’ coefficients (energy shift rates) from 0.5 to 3.5 meV/nm have been measured in good agreement with numerical calculations based on Picus–Bir orbital-strain Hamiltonian. For InAs/GaAs and InAs/AlAs

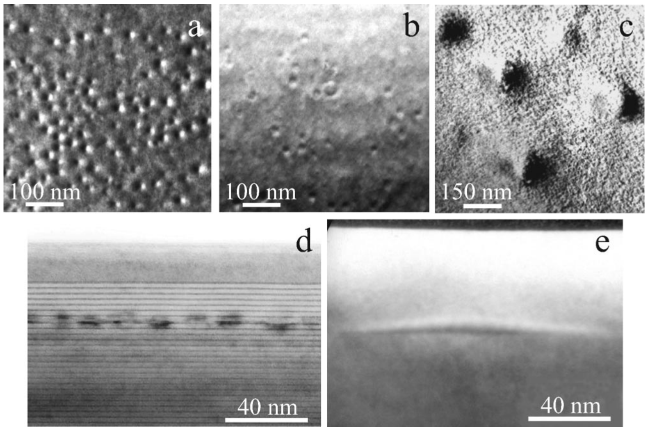

FIG. 1. (a)–(c) TEM planview micrographs of 2.4 ML InAs QDs (a) on AlAs and (b) on GaAs together with (c) 3 ML InP QDs on $Ga_{0.5}In_{0.5}P$. (d) and (e) are cross-sectional TEM images of InAs/AlAs and InP/GaInP structures, respectively.

QDs comparison of the experimental results with numerical analysis reveals a decrease of the energy shift rate due to a nonuniform In distribution. An anomalously strong lateral inhomogeneity of the local stress field has been observed. Our results demonstrate the use of NSOM for probing the local strain on the nanoscale, opening new possibilities to study properties of QDs. This has broader impact for high spatial resolution piezo-spectroscopy. The ability to control the emission properties of QDs using nanoindentation can be important for optoelectronic and quantum computing applications.

II. EXPERIMENTAL DETAILS

A. QD samples

We studied InAs/AlAs, InAs/GaAs, and InP/GaInP QD samples grown on [001] GaAs substrates. The QDs were obtained by strained layer epitaxy using the Stranski–Krastanov growth mode.[58,59] The formation of QDs was observed by transmission electron microscopy measurements presented in Figs. 1(a)–1(e). Samples for transmission electron microscopy (TEM) were prepared using standard mechanical polishing techniques with final Ar ion-milling, and studied in a 200 keV JEOL-2010FEG microscope. Plane-view samples were imaged presumably close to (022) two-beam conditions giving the highest strain contrast from QDs. The cross-sectional images were primarily taken using (200) dark-field conditions, which provide strong chemical contrast in this structure.

InAs/AlAs and InAs/GaAs QDs were formed by deposition of 2.4 monolayers (ML) of InAs within a short-period superlattice (SL) consisting of two/eight ML of AlAs/GaAs (average AlAs content 20%) by molecular beam epitaxy at 500 °C. The QDs, superlattice and 40 nm cap layer in the InAs/AlAs structure are clearly seen in cross-section image [Fig. 1(d)]. The InAs/AlAs QDs were grown on monolayers of AlAs within the SL described above, whereas InAs/GaAs QDs were grown on monolayers of GaAs, facilitating diffusion of AlAs or GaAs (respectively) into the dots. From TEM measurements [see Figs. 1(a), 1(b), and 1(d)] we found a bimodal distribution of dot sizes in both structures. There are larger dots having base ~15 nm and density 300(100) μm^{-2} for InAs/AlAs(InAs/GaAs) QDs and smaller ones having half of the size and density of large dots. The height of the dots is ~3–5 nm. We will show further that in our samples the bimodal distribution of dot sizes is accompanied with incorporation of Al or Ga into the QDs, which results in different InAs content for dots of different sizes, as was established from our near-field magneto-PL measurements to be described in the Appendix below. The mixing of the QD and matrix material is well established for strained layer epitaxy at high temperatures;[50] accounting for this mixing we will call our QDs as either InAlAs or InGaAs QDs instead of InAs QDs as is usually used in the literature. Moreover, we will distinguish the InAs QDs (higher InAs content) and InAlAs and InGaAs QDs (lower InAs content). It should be noted that a bimodal distribution of dot sizes is often observed for the deposition of ~1.7–2.5 ML of InAs (Refs. 51–53) or ~5 ML of InGaAs (Refs. 54–56) on GaAs. A theoretical argument for a bimodal size distribution for the InAs/GaAs system can be found in the thermodynamic equilibrium phase diagram of dense arrays of islands analyzed in Ref. 59. Some general speculations about the possibility of kinetically controlled bimodal distributions in InGaAs QDs are presented in Ref. 56.

InP QDs were grown at 700 °C by low pressure metalloorganic vapor phase epitaxy. Growth was started with the deposition of a 500-nm-thick $Ga_{0.5}In_{0.5}P$ lower barrier followed by nominally 3 ML of InP island deposition. After 5 s growth interruption the islands were overgrown by a 50-nm-thick upper $Ga_{0.5}In_{0.5}P$ [see Fig. 2(b)]. The dots have a base ~100 nm, density 20 μm^{-2} [see Fig. 1(c)] and height of 13 nm.

The structural and elastic[57] parameters of the QDs are summarized in Table I.

B. Near-field photoluminescence and indentation

The near-field photoluminescence (NPL) spectra were taken in collection-illumination mode at 10 K under excitation of the 514.5 nm Ar-laser line. The spectra were measured using a CCD detector together with a 280 mm focal length monochromator. The excitation power was 1–50 mW, which provided power density below the emission threshold of QD excited states (<20 W/cm^2). The spectral resolution of the system is 0.2–0.4 meV. We measured NPL spectra in a magnetic field up to 10 T, which allows us to estimate lateral dot sizes for specific emission lines.[22] A quarter waveplate and linear polarizer were used for separation of right- and left-hand circular polarization

An Oxford Instruments CryoSXP cryogenic positioning system was used for 3D scanning. Contact of the tip to a sample surface was controlled by a tuning fork and further increase of the vertical displacement (z) produces local pressure (nanoindentation) on the sample. A small micro-objective with focal length 5 mm attached to a fiber bundle was used to observe light coming from the tip outside the cryostat and thus to control probe stability. In near-field scan-

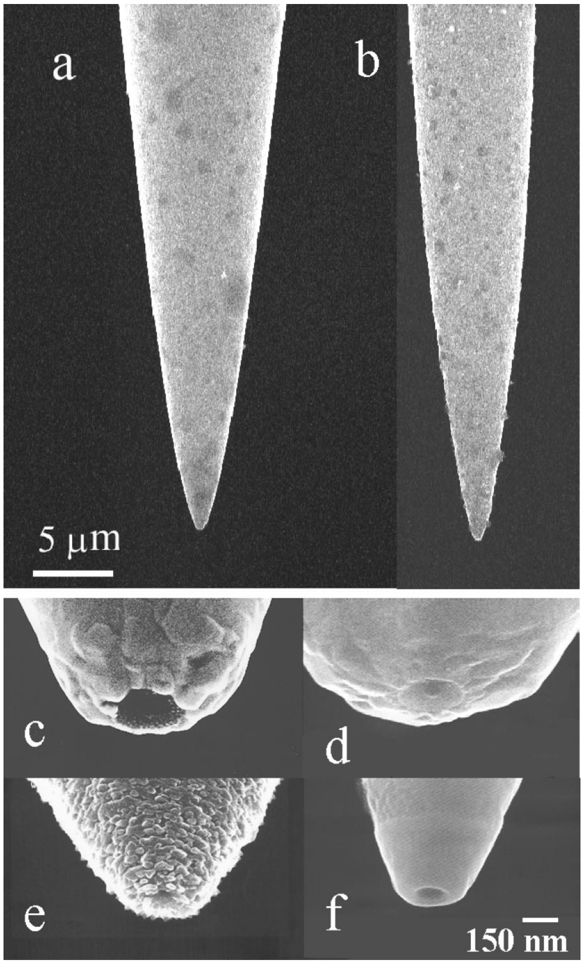

FIG. 2. SEM images of the near-field optical fiber probes: side view of the two types of tapers used (I-a, II-b); 45° tilt images of apertures having diameters (nm) and coating (see Table II for probe identification numbers): (c) 280 and Au (LAR22); (d) 270 and Al; (e) 60 and Al/Ti (L54); and (f) 120 and Al (PB82). The apertures were prepared by pulling (c), etching (d)–(f), and FIB trimming (f).

ning experiments the tip was positioned on ~5 nm above the surface. To locate the lateral position of the QDs we measured the intensity of the QD line in NPL spectra using several line *x*- and *y*-scans, with a step of 50 nm. The NPL spectra strongly decreases by moving the tip away from the sample. For coated tips (see below) the intensity decreases two–five times at distances 100 nm above the surface.

In nanoindentation experiments the spectra were recorded under increasing *z* (tip compression) above contact value by 7 nm steps. We use total vertical displacement up to 100 nm after which the tip was raised above the surface and then moved to another indentation point. This corresponds to the loading part of a standard nanoindentation experiment.[42] We also checked that the damage threshold of QDs (no recovery and reproducibility of the spectra after indentation) is ~300 nm. For some indentation points we observed a change the emission energy of a QD by several meV after unloading. However we also observed such changes of emission energy without pressure (tip above the surface) and ascribe these effects to light-induced spectral diffusion.[31]

NPL spectra at zero pressure and estimation of the InAs content and size for QDs from NPL measurements in the magnetic field are described in the Appendix.

C. Fiber probes

As near-field probes we used tapered single mode fiber tips coated by metal (Al or Au in combination with Ti) with thickness ~50–200 nm.[60] The physical structure of the aperture and its optical quality were controlled using scanning electron microscopy (SEM) imaging, visual observation of the light coming from the tip under a microscope with ×100 objective, and by measuring its far-field transmission for 632.8 nm wavelength (HeNe laser). The taper was prepared by using a pulling technique.[2,3] We used two pulling regimes in which the taper angle increases towards the tip end [see Figs. 2(a) and 2(b)]. Both regimes (hereafter referred as type I and II) give flat tips (apertures) with diameters >200 nm and aperture angles ~30°–40° [see Fig. 2(c)] but within a few micrometers from the aperture they have different taper angles (the angle is smaller for taper of type II). To make smaller apertures we used further chemical etching in a hydrofluoric acid solution.[10] We found that for long etching times, aperture diameters of 100–200 nm resulted, and the etching procedure produced apertures with small lenslike rounded bumps at the center, having bases ~50 nm [Fig. 2(d)]. We suppose that this happens due to a strong nonuniformity of the distribution of Ge at the SiO_2 taper cross section after pulling and resulting selective etching. For ap-

TABLE I. Structural and elastic parameters of QD samples.[a]

Matrix material	QD material	Density (μm^{-2})	Base (nm)	Young's modulus (Y) (kbar)	Poisson's ratio (ν)	Deformation potentials $a(-b)^{b}$ (eV)
GaInP	InP	20	100	820/611	0.34/0.36	6.5(1.8)
AlAs/GaAs	InAs	100	7	849/514	0.33/0.35	6(1.8)
	InGaAs[c]	50	15	849/652	0.33/0.34	7.3(1.9)
GaAs/AlAs	InAs	300	7	849/514	0.33/0.35	6(1.8)
	InAlAs[c]	150	15	549/652	0.33/0.34	7.3(1.9)

[a] Thickness of the cap layer is 40 nm for InAlAs and InGaAs and 50 nm for InP QDs.

[b] Reference 65.

[c] Parameters are given for 60% of InAs content.

TABLE II. Parameters of the near-field fiber probes used for nanoindentation.

Number	Probe identification number (taper -type)	Ending shape	Aperture diameter (nm)	Metal coating type (thickness, nm)	Transmission
1	L54(II)[a]	round	60	Al/Ti(50/50)	5×10^{-4}
2	PB71(II)	round	90	Al(80)	5×10^{-3}
3	PB82(II)	flat (FIB)	120	Al(90)	1.3×10^{-3}
4	L48(II)	bump	140	Al(100)	3×10^{-3}
5	S20(I)	flat	190	Al(80)	3×10^{-3}
6	L56(I)[a]	flat	260	Al(100)	10^{-3}
7	LAR22(II)	flat	280	Au(180)	3×10^{-3}
8	L61(I)[a]	flat	300	Al(200)	9×10^{-3}

[a] Indentation was done with metal coating removed.

erture diameters <100 nm the bump dominates the taper, leading to a rounded ending [Fig. 2(e)]. To produce flat apertures with diameters smaller than 200 nm we used a focused ion beam (FIB) milling technique[61] [Fig. 2(f)]. The transmission of our metal coated fiber probes was 10^{-4}–10^{-2}.

The metallic coating of the near-field tips plays an important role for achieving higher spatial resolution and light confinement at the aperture, but it complicates the numerical analysis of the stress. In our indentation experiments we were able to remove the metal coating from ~100 nm of the ending of the $\mathrm{SiO_2}$ core by using tip compressions >100 nm. Uncoated apertures made in this way have an order of magnitude higher light transmission but they have poorer spatial resolution and are less controllable.

We found that for most of the apertures the transmission does not change after ~20 indentations of <100 nm compression each, which indicates great stability of the metal coating. This allows us to use the same tip for measurements of three different samples. The parameters of the 8 fibers tips which were used in these nanoindentation experiments are presented in Table II.

III. CALCULATION OF INDENTATION-INDUCED ENERGY SHIFT OF QDS

A. Pressure-induced energy shift in III–V QDs

There are two contributions to the shift of the ground state energy of the QDs under stress, which arise form the modification of the band gap and the confinement potential. The modification of the band gap reflects changing of the bond lengths and angles (local symmetry) in strained material, while modification of the confinement potential reflects the changing of the band offsets between QD and matrix. We will neglect the latter contribution because the effect of strain on the energy bands of QD and matrix is similar. The strain-induced energy shifts of the band gap states in zinc blende semiconductors can be obtained using the Picus–Bir orbital-strain Hamiltonian for a given band at $k=0$,[62–64]

$$H_e(i) = -a^{(i)}(\varepsilon_{xx}+\varepsilon_{yy}+\varepsilon_{zz}) - 3b^{(i)}[(L_x^2-\tfrac{1}{3}\mathbf{L}^2)\varepsilon_{xx}+\text{c.p.}] - (6d^{(i)}/\sqrt{3})[\{L_xL_y\}\epsilon_{xy}+\text{c.p.}], \qquad (1)$$

where the superscript i is a band index, $\epsilon_{\alpha\beta}$ denotes the components of the strain tensor, $\mathbf{L}$ is the angular momentum operator, c.p. denotes cyclic permutations with respect to the indexes, x, y, and z, and the quantities in curly brackets indicate the symmetrized products, $\{L_xL_y\}=\frac{1}{2}(L_xL_y+L_yL_x)$. The parameter $a^{(i)}$ is the hydrostatic pressure deformation potential, and quantities $b^{(i)}$ and $d^{(i)}$ are deformation potentials appropriate to strains of tetragonal and rhombohedral symmetries, respectively. Using strain–stress relations the Hamiltonian (1) becomes[63]

$$\begin{aligned} H_e = &-a(S_{11}+2S_{12})(\sigma_{zz}+\sigma_{xx}+\sigma_{yy}) - 3b(S_{11}-S_{12}) \\ &\times[(L_z^2-\tfrac{1}{3}\mathbf{L}^2)\sigma_{zz}+\text{c.p.}] \\ &-(6d/\sqrt{3})S_{44}[\{L_xL_y\}\sigma_{xy}+\text{c.p.}]\}, \end{aligned} \qquad (2)$$

where S_{11}, S_{12}, and S_{44} are elastic compliance constants; $\sigma_{\alpha\beta}$ are stress tensor components; a, b, and d are the deformation potentials for the band gap between the Γ_{15} valance band and the Γ_1 conduction band.[65] Using in (2) the matrix elements of orbital momentum for heavy-holes tabulated in Ref. 66 we obtain the shift of the QD ground state energy induced by [001] compression to be

$$\Delta E_{e\text{-}hh} = \frac{a}{Y}(1-2\nu)(3\sigma^h) + \frac{2b}{Y}(1+\nu)\frac{3}{2}\sigma_{zz}^u, \qquad (3a)$$

or

$$\Delta E_{e\text{-}hh} = \frac{\sigma_{zz}}{Y}\left\{ a(1-2\nu)+b(1+\nu) + [2a(1-2\nu)-b(1+\nu)]\frac{\sigma_{rr}+\sigma_{\theta\theta}}{2\cdot\sigma_{zz}}\right., \qquad (3b)$$

where Y and ν are Young's modulus and Poisson's ratio, respectively, and $\sigma^h=\frac{1}{3}(\sigma_{zz}+\sigma_{xx}+\sigma_{yy})$ and $\sigma_{zz}^u=\sigma_{zz}-\sigma^h$ are mean and deviatoric[67] stress components, respectively. The expression (3b) is written in term of stress components in an axial coordinate system as σ_{rr} and $\sigma_{\theta\theta}$ $(\sigma_{rr}+\sigma_{\theta\theta}=\sigma_{xx}+\sigma_{yy})$, which is used below for numerical calculations. The two terms in expression (3a) are the shift of the band gap due to hydrostatic stress (δE_H) and the linear splitting of the light and heavy hole bands induced by [001] "uniaxial" stress (δE_{001}). For $\sigma_{xx}=\sigma_{yy}=0$ they coincide with corresponding quantities[64] for pure uniaxial stress. If $\sigma_{\alpha\beta}$ depends linearly on compression, the stress acting on a QD can be described by a shift rate parameter $S = \Delta E_{e\text{-}hh}/z$.

For III–V materials the deformation potential a (Ref. 65 and Table I) has values 6–10 eV, increasing with the increase of the material hardness and proportional to the Young's modulus. The deformation potential b has values near -2 eV, weakly depending on the material type. Thus the first (hydrostatic) term of Eq. (3a) is nearly independent of material parameters, while the second (uniaxial) term decreases with an increase of material hardness (increasing Y). Thus the total energy shift rate will increased with increasing Y.

As can be seen from expression (3b), for a given value of σ_{zz} the energy shift has a maximum value for pure hydrostatic stress ($\sigma_{zz}=\sigma_{rr}=\sigma_{qq}$) and a minimum for pure uniaxial stress ($\sigma_{rr}=\sigma_{qq}=0$). For the QD materials used in our experiments (Table I) the energy shift will have values between $(-5\cdot 10^{-4} - +10^{-2})\sigma_{zz}$ eV. The compression coefficient for typical SiO_2 near-field fiber probes can be estimated to be ~1 kbar/nm,[46] assuming no sample compression (i.e., the sample is much harder than the tip). Using factors of $\frac{1}{2}$ to account for the sample compression ($Y_{\text{SiO}_2}\approx Y_{\text{GaAs}}$) and the finite thickness of the cap layer one can obtain the energy shifts of a QD to be in the range from -2 to $+50$ meV for compression ~20 nm ($S\sim -0.1 - +2.5$ meV/nm), which is within an order of magnitude agreement with the energy shifts reported in Refs. 46–49. Below we will use finite element modeling to calculate the stress components of expression (3b), allowing us to make a direct comparison with the experiment and analyze the effect of the probe and material properties on the energy shift of QDs.

B. Finite element modeling of the local stress and energy shift rate for a QD

A two-dimensional axisymmetric finite element model was developed to calculate stress components. A computation domain containing four-node bilinear elements was constructed for the sample and the fiber tip. The element type was CAX4 in ABAQUS. The number of elements ranged from 4500 to 6900 while that of nodes ranged from 4722 to 7162. The mesh was optimized in terms of convergence of the results (accuracy) and calculation time. The resulting accuracy of the stress values 10 nm away from the stress singularities was estimated to be within 20%, which is suitable for comparison with experiment. The flat tip was simulated as a tapered cylinder with taper angle of 40°. The rounded tip was simulated by a parabolic curve $y=x^2/60$, measured using SEM images. The length of the tip (16 000 nm) was chosen from the finite element simulations from the condition of convergence of the tip displacement in contact with the sample, which is 0.29 of the total displacement. Due to the axial symmetry, only one QD can be inserted in the model, and it must be along the axis. We did not model the metal coating. Indentation was simulated assuming the tip presses directly into the top surface of the structure.

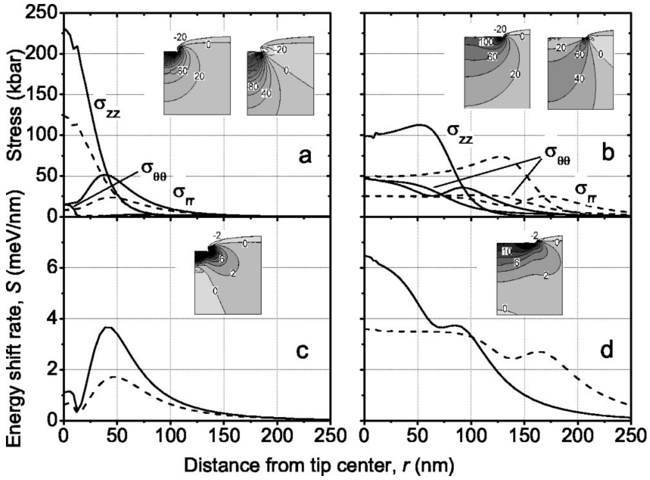

FIG. 3. Lateral distribution of the stress components (a and b) and corresponding energy shift rate (c and d) in a QD layer for an InGaAs dot for tip compression 70 nm and for: rounded (dashed curves) and 50 nm flat (solid curves) tips (a) and (c); 150 (solid curves) and 300 nm (dashed curves) tips (b) and (d). Inserts show contours of hydrostatic (left) and uniaxial (right) stress for 50 (a) and 150 (b) nm tips and corresponding contours of energy shift rates (c and d). For the insert the horizontal scale is $0\leqslant r \leqslant 100$ nm.

The calculations have shown that the stress components depend linearly on tip compression. This allows us to use compression coefficients $\sigma_{\alpha\beta}/z$ to characterize indentation properties of the tips, and a shift rate parameter S to characterize the stress in QDs.

In Fig. 3(a) we show the lateral distribution of the stress components (tip compression 70 nm) in the InGaAs QD layer calculated for tips having rounded and 50 nm diam (D) flat apertures, and in Fig. 3(b) we show the results for tips having 150 and 300 nm flat apertures. Inserts in Figs. 3(a) and 3(b) show contours of the hydrostatic(mean) and uniaxial(deviatoric) stress for $D=50$ and 150 nm, respectively, for contact region after indentation. Note that the horizontal scale of the insert cover ~100 nm, and can be determined by the radii of the indented regions [25 and 75 nm for (a) and (b), respectively]. Simultaneously Figs. 3(c) and 3(d) show the lateral distribution of the energy shift rate $S(r)$ and its contours (inserts) calculated from data in Figs. 3(a) and 3(b) using expression (3b). One can see that the stress components decay strongly beyond the contact area ($r>D/2$). Under the tip ($r<D/2$) the stress has predominantly uniaxial character ($\sigma_{zz}\gg\sigma_{rr}$) for rounded and 50 nm flat apertures, while it has relatively stronger hydrostatic character ($\sigma_{zz}\sim\sigma_{rr}$) for 150 and 300 nm apertures. The increase of the vertical stress (σ_{zz}) with decreasing D is due to the concentration of the stress singularity at the tip edges [compare the insert in Fig. 3(a) with 3(b)]. Stress singularity can also be seen as a sharp discontinuity at a QD edge at $r\sim 10$ nm and depth 40 nm. Due to elimination of the edge stress the rounded tip has two times smaller stress compared with the 50 nm flat aperture. At $r\sim 0$ the vertical stress (σ_{zz}) decreases as $\sim 1/D$, while the lateral stress (σ_{rr} and σ_{qq}) has a maximum at $D\sim 150$ nm.

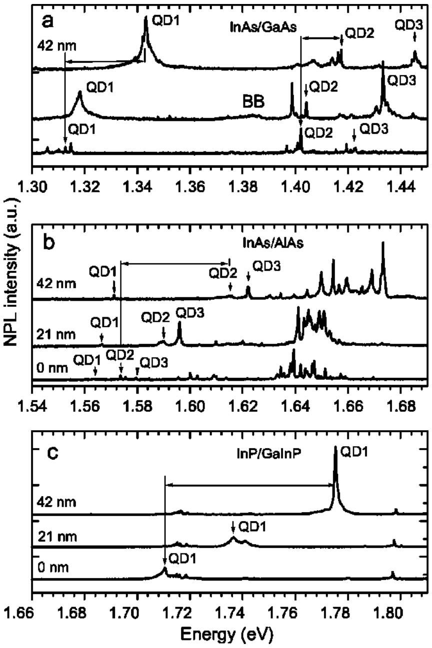

FIG. 4. NPL spectra of InGaAs (a, 120 nm tip), InAlAs (b, 120 nm tip), and InP QDs (c, 200 nm tip) and for tip compressions $z = 0$, 21, and 42 nm.

The energy shift rate distributions [Figs. 3(c) and 3(d)] show similar decaying behavior beyond the tip as the corresponding stresses in Figs. 3(a) and 3(b). For 150 and 300 nm apertures a local maximum due to an increased hydrostatic component is seen at the tip edges. For rounded and 50 nm flat apertures the shift rate is close to zero near the tip center due to the predominantly uniaxial character of the stress. The energy shift rate has values 3.8 meV/nm for 50 and 300 nm tips and 6.2 meV/nm for the 150 nm tip. The higher value of S for the 150 nm tip reflects the compromise between the decrease of the vertical stress and the increase of the hydrostatic contribution as D increases. Dividing the values of stress components acting on the QD (at 40 nm from the sample surface) presented in the inserts in Figs. 3(a) and 3(b) by the value of tip compression (70 nm) one can relate the energy shift rate values to compression coefficients of the hydrostatic(uniaxial) stress components as 1.1(2) and 0.86(0.57) kbar/nm for 50 nm and 150 nm tips, respectively. The rounded tip has one-half the S values and compression coefficients. From inserts in Figs. 3(c) and 3(d) one can see that S values [as well as the stress components in the inserts in Figs. 3(a) and 3(b)] strongly decay away from the surface in the vertical direction. They have maximum values ($\sim$10 meV/nm) at the surface, and decrease down to negative values $\sim$1 meV/nm for $z > D$.

IV. NEAR-FIELD PL SPECTROSCOPY OF SINGLE QDS UNDER NANOINDENTATION

A. NPL spectra

In Figs. 4(a)–4(c) we present selected spectra of our InAs/GaAs, InAs/AlAs, and InP/GaInP samples showing the behavior of the single QD emission lines under indentation by the near-field optical fiber probe. The main effect here is a strong high energy shift with increasing z as was reported previously.[46–49] The lines also broaden. For InAs, InGaAs, and InAlAs QDs in InAs/GaAs and InAs/AlAs structures (see Appendix) this increased halfwidth does not exceed 1 meV in most cases, but there are a few cases for which the broadening is much greater [up to 6 meV for QD1 in Fig. 4(a)]. For InP QDs the halfwidth can increase up to 10 meV. It should be mentioned that under indentation of InAs/GaAs and InAs/AlAs QD structures we also observed the appearance of very broad bands with halfwidth up to 20 meV [BB band in Fig. 4(a)], which cannot be related to a specific QD. Such bands often show much higher energy shifts, which suggests a possible connection with light-hole transitions.

We also observed a strong increase (up to one order of magnitude) of the emission intensity of single QD lines under indentation [QD1 and QD3 in Fig. 4(a), QD3 in Fig. 4(b), and QD1 in Fig. 4(c)]. Our preliminary study shows no direct correlation of the intensity increase with the amount of pressure produced by the tip, nor with the increased coupling of near-field radiation to the aperture, resulting from decreased distance between tip and dot.[68] Moreover such an increase is absent for uncoated tips (see below). We propose that the increase is connected with the deformation of the metal coating which increases the coupling of light with surface plasmons at the aperture.

From Fig. 4 one can see that for a compression of 42 nm the energy shift is 30–40 meV for InAs QDs [QD1 and QD2 in Figs. 4(a) and 4(b), respectively] and 60 nm for InP QDs [QD1 in in Fig. 4(c)]. The InGaAs and InAlAs QDs [Figs. 4(a) and 4(b)] show smaller shifts ($<$20 meV). In our present experiments we observed an energy shift as much as 150 meV for compressions up to 50 nm. These observed shifts correspond to the S values 1–3 meV/nm, which give an order of magnitude agreement with calculations presented in Figs. 4(c) and 4(d). However to make comparison between experiment and calculations more reasonable one needs to check the linear dependence of the energy shift on tip compression (no plastic deformation), specify the distance between the indentation point and the QD and account for the metal coating. We shall attempt to do so below.

B. Energy shift of QD emission lines

The dependence of the energy of the ground state emission line of a single QD (E_{gs}) on tip compression (z) is a spectroscopic analog of the nanoindentation load-displacement curve in mechanical systems.[42] We found that the shape of the $E_{\mathrm{gs}}(z)$ curve depends on the presence of the metal coating and lens-shape bump at the aperture ending. Contour plots representing a set of the spectra taken for different compressions are shown in Figs. 5(a)–5(c) for three types of apertures: (a) coated flat, (b) uncoated flat, and (c) coated nonflat [with rounded bump at the ending of Fig. 2(d)]. In the figure the $E_{\mathrm{gs}}(z)$ dependence can be traced by curves created by bright dashes corresponding to the emission energy of individual QD lines at various values of z. The gray scale shows the emission intensity. We can see that for coated apertures [(a) and (c)] the intensity of single QD lines

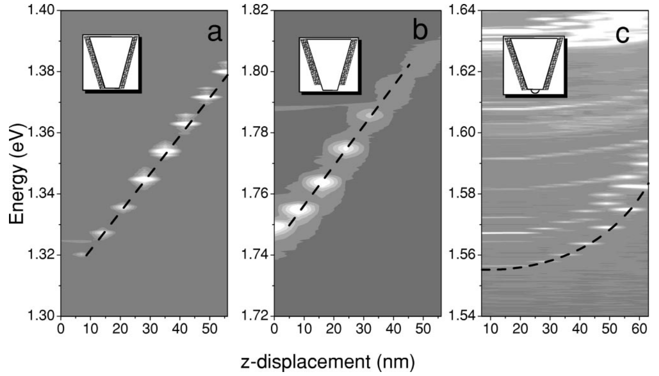

FIG. 5. Dependence of near-field PL spectra (3D contour plot) on tip compression. The aperture type (see inserts) and size (number), and the QDs are (a) coated, 120 nm (PB82) and InGaAs; (b) uncoated, 260 nm (L56) and InP; (c) coated/nonflat, 130 nm (L48) and InAlAs. Dashed lines are drawn for clarity.

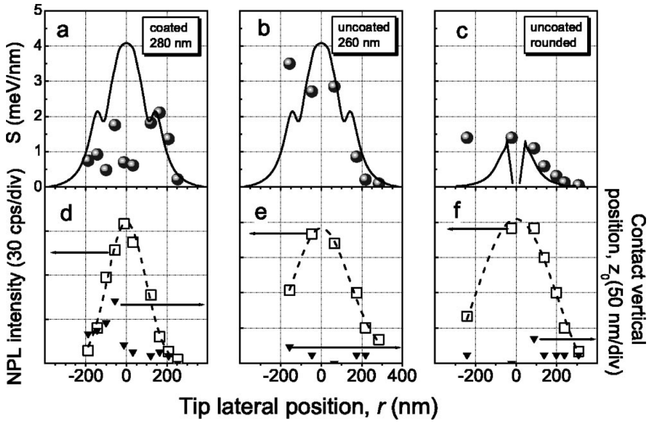

FIG. 6. Measured InP QD shift rate (S) values (circles in a–c), zero pressure QD line intensity (squares in d–e) and contact vertical displacement values (triangles in d–e) at different tip locations (r) for fiber LAR22 (a and d, 280 nm, Au coated), L56 (b and e, 260, uncoated), and L54 (c and f, rounded, uncoated) tips (see Table I). Solid curves are calculated results for 250 nm flat (a and b) and rounded (c) tip; dashed curves in d–f are Gaussian contour fitting.

increases strongly under indentation, as was mentioned above, but for the uncoated aperture (b) it decreases.

A linear $E_{\mathrm{gs}}(z)$ dependence is observed in Fig. 5(a) for the flat coated aperture. We found that the rounded coated aperture as in Fig. 5(e) also gives a linear dependence. For the uncoated aperture the dependence is close to linear at compressions up to 30 nm and then the slope decreases [Fig. 5(b)]. The change of the slope at high compression reflects the fact that the metal coating comes in contact with the sample, which reduces the contact force. There are also initial contact nonlinearities ($z < 10$ nm), which often take place for the coated tips. The nonflat aperture has a strongly nonlinear $E_{\mathrm{gs}}(z)$ curve with increasing slope. We did not use these apertures further in our nanoindentation experiments.

Our observation of the linear dependence of the energy shift on tip compression agrees very well with numerical calculations for flat and rounded apertures. The linear dependence indicates that no plastic deformation of the QD occurs under the indentation of the near-field probe for compressions up to 50–70 nm. This agrees qualitatively with nanoindentation experiments using a diamond Berkovich pyramid, in which a threshold depth (load) for the plastic deformation of III–V compounds was found to be 20–30 nm (200 μN).[69,70] In our experiment the significantly higher plastic deformation threshold which we observed results from the QD position 40–50 nm below the surface, and from the lower stiffness of the quartz core of the fiber.

C. Lateral distribution of local strain in QD structures

We used $E_{\mathrm{gs}}(z)$ dependencies measured at different tip locations to study the lateral distribution of the energy shift rate values. In these experiments the emission of a single QD is used as a local probe of the stress field produced by the near-field fiber tip. In these experiments the lateral distance between the QD and the tip (r) can be specified and thus direct comparison between calculated (Fig. 3) and experimental $S(r)$ distributions can be made. In Figs. 6(a)–6(c) we present experimental and calculated $S(r)$ data for InP QDs, for a coated 280 nm flat aperture and for two uncoated apertures: 260 nm flat and rounded. In Figs. 6(d)–6(f) we plot the corresponding zero pressure emission intensity together with the contact value of the vertical displacement (z_0) to monitor the aperture stability and surface roughness.

The data from Figs. 6(d)–6(f) reveal that in a sequence of several successive nanoindentations of a single QD, its zero pressure emission intensity follows a distinct Gaussian-type lateral distribution, which demonstrates both aperture stability and the reversibility of the spectra. This agrees with the linear $E_{\mathrm{gs}}(z)$ dependence [Fig. 5(a)] and absence of the plastic deformation. These results clearly demonstrate that we can measure the space QD position and r values. The data show higher spatial resolution for the metal coated aperture ($\sim$200 nm) compared with uncoated tips ($\sim$300 nm). The spatial resolution for uncoated tips, 300 nm, agrees with results of Refs. 28 and 71.

At the same time the contact value z_0 shows strong lateral variations—up to 70 nm in Fig. 6(d) and up to 30 nm in Figs. 6(e) and 6(f). Such variations cannot reflect surface roughness, as this contradicts the line intensity behavior. Indeed, the strong dependence of the NPL intensity on the vertical displacement observed for the tip positioning above the surface (up to five times intensity decrease for $\Delta z \sim +100$ nm for coated tip), cannot lead to a smooth Gaussian-type shape of the intensity curve assuming that $z_0(r)$ is related to the surface roughness. We can therefore assume that the strong lateral variation of z_0 is due to some attractive forces between the tip and the sample, which cause the moving of materials under the contact area after the indentation, leaving the distance between the QD and sample surface (thickness of the cap layer) unchanged. We suppose that these forces depend on the roughness of the sample and the tip (metal coating). The strong lateral inhomogenitiy of such forces can explain the anomalously strong lateral variation of the shift rate value in Fig. 6(a), which is not predicted by the calculations. It can be seen from Fig. 6(a) that S (and hence the stress values) changes several times at $r \sim 50$–100 nm, being

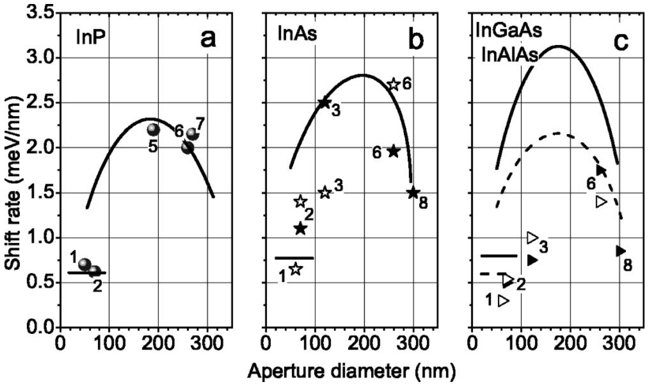

FIG. 7. Values of the shift rate vs aperture diameters of coated tips for (a) InP (solid circles), (b) InAs on GaAs (open stars) and InAs on AlAs (solid stars) and (c) InGaAs (open triangles) and InAlAs (solid triangles) QDs. Solid lines are calculations for uncoated tips divided by a factor of 2: curves are for flat tips and horizontal straight line are for rounded tips. The curves are quadratic polynomial approximations of discrete calculated points. Dotted curve in c is the calculation accounting for nonhomogenity of the InAs distribution (see text). Numbers near experimental points denote tip types from Table I.

minimum near the QD center. We also observed similar nonregular variations of $S(r)$ for InAs, InGaAs, and InAlAs QDs, as was reported in our preliminary study.[68]

As can be seen in Figs. 6(b) and 6(c), smaller z_0 variations result in smoother behavior of the $S(r)$ curves. Here a gradual decrease of the shift rate with increasing r can be observed for some direction (for $r>0$), but is nonmonotonic for the others ($r<0$).

In Figs. 6(b) and 6(c), for the smooth parts of the $S(r)$ curves (i.e., $r>0$) the agreement between experiment and calculation is very good. The calculations agree with the experimental result that the maximum shift rate for a rounded aperture (1.5 meV/nm) is approximately half of that measured for the ~260 nm aperture (3.5 meV/nm). We should point out that no adjustable parameters have been used in the calculations. We feel that these are extraodinary results, showing that we can reproducibly produce known amounts of strain (in agreement with calculations) repeatably, using various tips of glass fibers that have been prepared in our laboratory.

Below we will use maximum shift rate values obtained from $S(r)$ data for different fiber tips to the study dependence of the shift rate values on aperture diameter.

D. Effect of aperture size on the energy shift of QDs

In Figs. 7(a)–7(c) we present shift rate values for InP, InAs, and InGaAs and InAlAs QDs measured with different aperture sizes. We should point that each set of data points has been measured twice with the same tip, to eliminate possible uncertainties in the measurements due to scatter of the indentation properties of different tips. In this figure we also show calculated results for uncoated apertures, divided by a factor of 2 to adjust to the fact that the fibers used were coated, as described below. We also used the same factor for data in Fig. 7 taken with uncoated tips. We obtained this factor by comparing of the S values for coated and uncoated tips with the same apertures [see, for example, Figs. 6(a) and 6(b) and Fig. 7(a) for ~250 nm apertures and Figs. 6(c) and 7(a) for rounded apertures]. The physical meaning of this factor can be a renormalization of the contact force. A decrease of the contact force indicates that the metal coating acts as a soft shell, i.e., it has lower stiffness and can slide along the tip core.

The calculated curves show that for flat apertures the energy shift has maximum values at tip diameters 150–200 nm, which reflects the compromise between the decrease of the vertical stress and the increase of the hydrostatic contribution as D increases, as was described above. The S values of rounded apertures is one-half of the 50 nm flat ones. For similar aperture sizes the calculated S values are ~20% smaller for InP and ~10% higher for InGaAs(InAlAs) QDs compared with the InAs QDs. These differences result from the thicker cap layer (50 nm) of InP/GaInP structure and the greater hardness of InGaAs(InAlAs) QDs, respectively.

For InP QDs [Fig. 7(a)] the measured S values for all tips used (~0.7 meV/nm for rounded tips and ~2.1 meV/nm for 200–280 nm tips) coincide with the calculated values within 10%.

For InAs QDs [Fig. 7(b)] the agreement is also good but for one rounded tip (PB71; number 2 in the figure) and the 120 nm flat tip (PB82; number 3 in the figure) the measured S values differ from the calculated ones by 1.5 times. Such scatter of the measured shift rate values can be attributed to the high dot density, i.e., high elastic inhomogenity, of these QD structures, which results in stronger elastic interactions between neighboring dots.

For InGaAs and InAlAs QDs the agreement is poor; all measured values are much lower (up to two times) than the calculated ones. Our analysis has shown that the strong reduction of the S value for these QDs can be attributed to the reduction of the hydrostatic pressure coefficient $P_h = 3a(1-2\nu)/Y$ [first term in expression (3a)] due to the nonuniform In composition, resulting in the localization of the exciton in the central InAs-rich region of the QD. Such localization, established from our magneto-NPL measurements (see Appendix), reduces the effective hydrostatic deformation potential a (higher In concentration) and will decrease P_h, as well as S, assuming that the elastic properties (Young's modulus) are determined by the "physical" QD volume (lower In concentration). Revised calculations, which qualitatively account for this effect are presented in Fig. 7(c) by the dotted line; these results show better agreement with experiment. It should be noted that the reduction of the hydrostatic pressure coefficient was observed experimentally for InAs/GaAs (Refs. 72, 73) and InAlAs/AlGaAs (Ref. 74) QD ensembles.

We should point that the overall good agreement between calculated and experimental S values gives strong evidence that such instrumental factors as the difference in taper type (tips of type I and II), deviation from exact right-angle indentation conditions (difference in contact area), bending of the tip, friction between tip and sample, etc. give small contributions on the measured S values in our QD structures.

The overall good agreement between calculated and experimental *S* values allows us to evaluate, from these calculations, the compression coefficients ($\sigma_{\alpha\beta}/z$) for the tip-induced hydrostatic(uniaxial) stress components acting on QDs in our structures, i.e. at the depth of 40 nm for InAs/GaAs and InAs/AlAs structures and 50 nm for the InP/GaInP structure. For coated tips which is favorable for high spatial resolution near-field spectroscopy, these coefficients are ~0.6(1), ~0.4(0.3), and ~0.2(0.2) kbar/nm for flat apertures having diameters 50, 150 nm tip and 300 nm, respectively. For rounded tips they are ~0.3(0.5) kbar/nm. Higher compression coefficients and energy shift rates values can be obtained in self-organized QD structures with very thin cap layers (~10 nm). In nanoindentation experiments using optical fiber near-field probes, extremely large shifts of the QD ground state energy (up to 0.5–1 eV) can be achieved in such structures. For such structures much higher spatial resolution (~30 nm) can be obtained allowing one to study the effect of tip-induced pressure on the excited and multiexciton states of a single QD.

V. CONCLUSION

In conclusion we studied the emission spectra of single self-organized InAs, InGaAs, InAlAs, and InP QDs using low-temperature near-field photoluminescence. We investigated the dependence of these spectra on the local pressure produced by the optical fiber probe (nanoindentation). A high energy shift (up to 150 meV), broadening (up to 10 meV), and intensity increase (up to one order of magnitude) of the single QD emission lines have been observed at tip compressions of 30–70 nm. "Pressure" coefficients (energy shift rates) from 0.5 to 3.5 meV/nm have been measured for different aperture types (rounded and flat, metal coated and uncoated) and sizes (50–300 nm), in good agreement with finite element analysis. It was shown that the observed shift rate values reflect the interplay of hydrostatic(mean) and uniaxial(deviatoric) stress components under indentation of the near-field probe and correspond to tip-induced compression coefficients of 0.2–1 and 0.2–2 kbar/nm, respectively. For InGaAs and InAlAs QDs comparison of the experiment and numerical analysis shows a decrease of the energy shift rate due to the nonuniform In distribution. Anomalously strong lateral inhomogeneity of the local stress field has been observed. The reproducibility of these results, and the agreement between theory and experiment obtained in this study, demonstrate the possibility for using the NSOM fiber to probe local strain on the nanoscale, which opens up new possibilities for studying the properties of QDs. The ability to control the emission properties of QDs with local strain can be important for optoelectronic and quantum computing applications.

ACKNOWLEDGMENTS

The authors wish to thank Sergei Osinski, Pavel Blagnov, and Valeri Larionov for fiber fabrication, Yri Musikhin for TEM measurements of InP/GaInP structure, and Alexander Govorov for helpful discussions of theoretical results. Support for these investigations was provided by the W. M. Keck Foundation, the DARPA/ONR Grant No. N00014-01-1-0658, by the NSF Materials Research Science and Engineering Center for Nanoscopic Materials Design at the University of Virginia and Notre Dame, and by the MACRO-DARPA Focus Center for Interconnects for Gigascale Integration at the State University of New York at Albany.

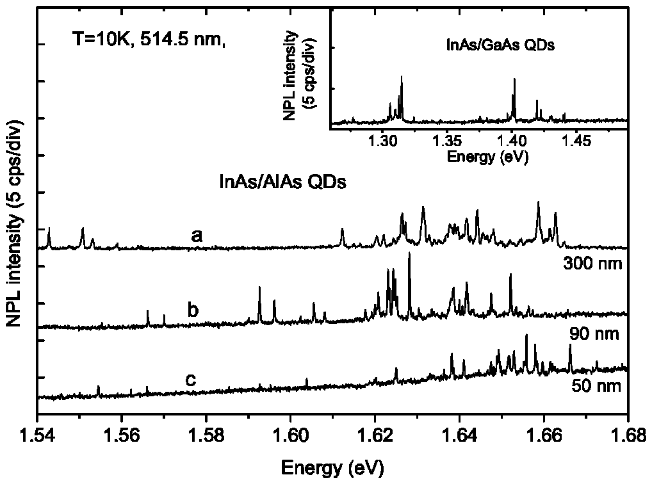

FIG. 8. Low-temperature NPL spectra of InAlAs QDs taken with tips having aperture diameter (transmission), nm: (a) 300 (10^{-2}); (b) 90 (5×10^{-3}); and (c) 50 (5×10^{-4}). Insert shows the spectra of InGaAs QDs taken with fiber tip diameter 140 nm (2×10^{-3}).

APPENDIX: CHARACTERIZATION OF THE QDS USING NEAR-FIELD MAGNETO-PL SPECTROSCOPY

1. InAs/AlAs and InAs/GaAs QDs

In Fig. 8 we present the near-field photoluminescence (NPL) spectra of InAs/AlAs QDs; insert shows the spectra from InAs/GaAs QDs. For InAs/AlAs QDs the spectra were taken with three fiber probes having aperture diameter 50, 90, and 300 nm. The spectra consist of a number of sharp lines (up to twenty) corresponding to ground state emission of single QDs. The halfwidth of the sharp lines is equal to the spectral resolution of our setup (0.2–0.4 meV). The number of lines depends weakly on the aperture diameter and for a dot density 300 μm^{-2} corresponds to a spatial resolution ~200 nm. Scans of the line intensities also give a value of 200 nm. This spatial resolution is much poorer then expected for the 50 and 90 nm aperture diameters used and can be attributed to a lateral spreading of the near-field component in the 40 nm thick cap layer.[75]

The lines are observed at energies 1.50–1.7 eV for InAs/AlAs and 1.3–1.45 eV for InAs/GaAs QDs. We attribute this difference in the emission energy of InAs/AlAs and InAs/GaAs QDs with the differences of the band-gap energy of the matrix material. We can also see that for each sample the lines are grouped in two distinct energy ranges separated by 100 meV (1.55 and 1.64 eV for InAs/AlAs and 1.31 and 1.42 eV for InAs/GaAs QDs), which reflects the bimodal distribution of dot sizes.

In Fig. 9 we present the observation of the Zeeman split-

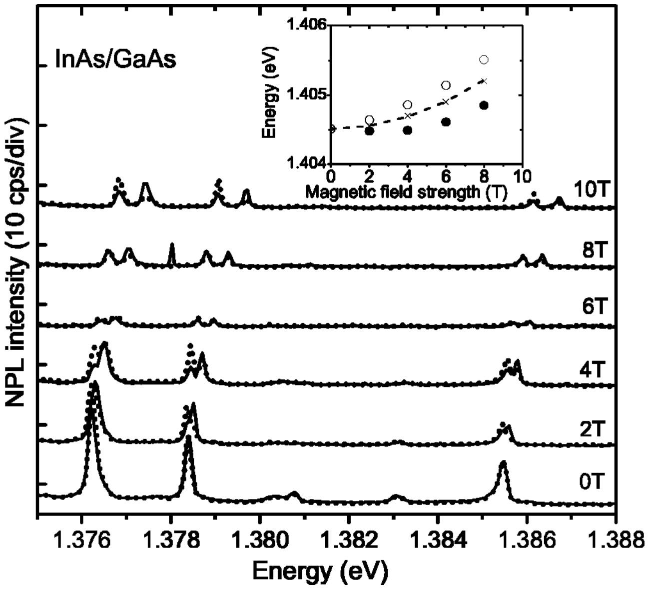

FIG. 9. $\sigma-$ (solid) and $\sigma+$ (dotted) circularly polarized components of the NPL spectra of InGaAs QDs measured at magnetic field strengths 0, 2, 4, 6, 8, and 10 T. Insert shows dependence of the energy of $\sigma-$ (solid circles) and $\sigma+$ (open circles) components and their average value (cross, experiment; dashed curve, quadratic approximation) vs magnetic field strength for one particular QD.

ting and diamagnetic shift for InAs/GaAs QDs in a magnetic field. Each line observed in the spectra splits into $\sigma+$ and $\sigma-$ circular polarized components in the magnetic field, and thus corresponds to different QDs.

We found that the diamagnetic coefficient (β) has different values for two sets of emission energy ranges of InAs/AlAs and InAs/GaAs QDs [see Figs. 10(a) and 10(b)]. For low emission energy β has nearly constant values ~4 and ~7 μeV/T^2 for InAs/AlAs and InAs/GaAs QDs, respectively. For higher emission energies β gradually increases, reaching values 10 μeV/T^2 for InAs/AlAs QD and 15 μeV/T^2 for InAs/GaAs QDs. For InAs/AlAs QDs the increasing diamagnetic coefficient, which corresponds to an increase of the dot size, correlates well with decreasing Zeeman splitting (from ~1 to 0.5 meV at 10 T).[76] For InAs/GaAs QDs the Zeeman splitting (0.2–0.7 meV at 10 T) depends only weakly on the energy. Using these measured values of the diamagnetic coefficient and the value of exciton effective mass 0.053 (Refs. 77–79) we calculated the lateral size of InAs/GaAs and InAAs/AlAs QDs as was described in Ref. 22. The calculated dot sizes are plotted in Figs. 10(c) and 10(d). They agree well with TEM data from Table I for low emission energy (small QDs) but for high emission energy the diamagnetic shift gives 30% smaller values, as indicated by horizontal arrows.

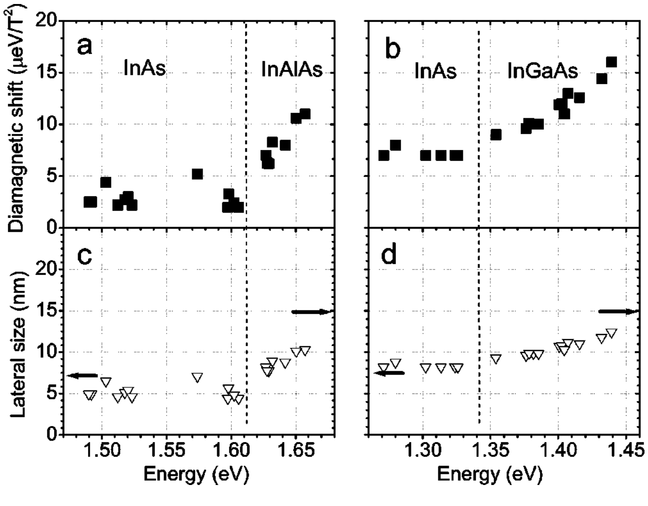

FIG. 10. Diamagnetic shift (a and b) and lateral size (c and d) of InAlAs (a, c) and InGaAs (b, d) QDs vs emission energy. Horizontal arrows in c and d show dot base measured from TEM data. Vertical dashed line separates emission energies of different size dots.

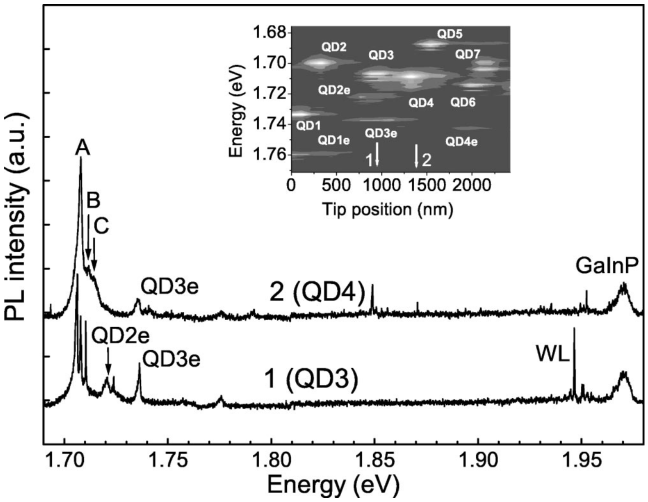

FIG. 11. Low-temperature NPL spectra of InP QDs taken at 1 and 2 tip positions of spatially and spectrally resolved NPL scan (left insert).

Our observation of increasing QD size with increasing emission energy is quite unexpected[56] and implies lower In content for larger dots, which compensates the usual quantum confinement effects. According to eight-band $\mathbf{k}\cdot\mathbf{p}$ calculations,[80] a change of InAs QD base dimension from 10 to 20 nm leads to a decrease of the confinement energy of 200 meV. Thus smaller dots having ~100 meV lower emission energy have ~300 meV lower band gap. Taking into account the change of the band gap of InGaAs by ~100 meV per 10% of In,[81] and the change of the exciton energy by 70 meV with a change of the In composition by 10% in InGaAs QDs (from 50% to 60%) obtained from first principles calculations,[82] one can estimate the difference in In composition in the small and large QDs to be 30% or 40%. Accounting for this difference we will henceforth refer to the small dots as InAs QDs and to the large ones as InGaAs or InAlAs QDs. Accordingly we used InAs composition values of 100% and 60%, respectively, for the material parameters presented in Table I.

The smaller QDs sizes obtained from diamagnetic shift measurements compared with TEM measurements indicate that excitons are localized on only a part of the "physical" volume of the dot. Such localization can occur at the central region of the dot, where higher In concentration has already been well documented for InGaAs QDs.[82–84]

2. InP QDs

In Fig. 11 we present the near-field emission spectra of individual InP QDs. In the left upper insert we show spatially and spectrally resolved near-field PL intensities plotted using a set of spectra taken at 10 tip positions along a line. This allows the determination of individual QDs (QD-QD7, QD1e-QD4e). The spectra in Fig. 6 were taken when the tip was located on QD3 and QD4 (positions 1 and 2 in the insert). We see that the emission of a single QD dominates each spectra due to the low density of QDs in this sample. The spectra of InP QDs contains a strong emission manifold at ~1.71 eV related to a central QD, weak manifolds at 1.7–1.79 eV related to the QDs located close to the tip edge (QD2e and QD3e), ultranarrow lines (with halfwidth $\gamma \sim 0.2$ meV) from the wetting layer (WL) centered at 1.95 eV and the GaInP matrix band at ~1.97 eV ($\gamma = 15$ meV). The QD density estimated from these data is $\sim 2 \times 10^9$ cm^{-2}, which agrees well with TEM data [Fig. 1(c)].

Inspecting the spectra of ~25 QDs we found that in most cases the emission manifold of the single InP QD has three components, denoted as A, B, C, having halfwidths of 3–5 meV and energy splitting of 4–15 meV (QD4). For some dots we found a fine structure of the components consisting of a several ultranarrow lines with $\gamma = 0.2$ meV (QD3). For these dots, the splitting between the A, B, and C components reduces to values as small as 1–2 meV. Several meV halfwidth and multiple peak structure with splitting up to 20 meV is the intrinsic feature of the low-temperature emission of single InP/GaInP QDs independent of their sizes.[19,85,86] The energy splitting of up to 20 meV of the emission manifold in InP/GaInP QDs can be attributed to quantized heavy hole levels.[87]

---

[1] E. H. Synge, Philos. Mag. **6**, 356 (1928).

[2] D. W. Pohl, W. Denk, and M. Lanz, Appl. Phys. Lett. **44**, 651 (1984).

[3] A. Lewis, M. Isaacson, A. Harootunian, and A. Muray, Ultramicroscopy **13**, 227 (1984).

[4] U. C. Fischer and D. W. Pohl, Phys. Rev. Lett. **62**, 458 (1989).

[5] D. Coutjon, K. Sarayeddine, and M. Spajer, Opt. Commun. **71**, 23 (1989).

[6] R. C. Reddick, R. J. Warmack, and T. L. Ferrell, Phys. Rev. B **39**, 767 (1989).

[7] E. Betzig and J. K. Trautman, Science **257**, 189 (1992).

[8] Daniel Courjon, *Near-Field Optics*, NATO ASI Series E: Applied Sciences, in Proceedings of NATO Advance Research Workshop on NFO, 26–28 October 1992, edited by D. W. Pohl (Kluwer Academic, Dordecht, 1993).

[9] M. A. Paesler and P. J. Moyer, *Near-Field-Optics* (Wiley, New York, 1996).

[10] M. Ohtsu, *Near-Field Nano/Atom Optics and Technology* (Springer-Verlag, Tokyo, 1998).

[11] S. K. Buratto, Curr. Opin. Solid State Mater. Sci. **1**, 845 (1996).

[12] B. Hecht, B. Sick, U. P. Wild, V. Deckert, R. Zenobi, O. Martin, and D. Pohl, J. Chem. Phys. **112**, 7761 (2000).

[13] H. Heinzelmann and D. Pohl, Appl. Phys. A: Solids Surf. **59**, 89 (1994).

[14] R. C. Dunn, Chem. Rev. (Washington, D.C.) **99**, 2891 (1999).

[15] Ch. Lienau and T. Elsaesser, *Ultrafast Physical Processes in Semiconductors* (Academic, Boston, 2001), Vol. 67.

[16] J. W. P. Hsu, Mater. Sci. Eng., R. **R33**, 1 (2001).

[17] Y. Toda, M. Kourogi, M. Otsu, Y. Nagamune, and Y. Arakawa, Appl. Phys. Lett. **69**, 827 (1996).

[18] F. Flack, N. Samarth, V. Nikitin, P. A. Crowell, J. Shi, J. Levy, and D. D. Awschalom, Phys. Rev. B **54**, R17312 (1996).

[19] G. Guttroff, M. Bayer, A. Forchel, D. V. Kazantsev, M. K. Zundel, and K. Erbel, Phys. Status Solidi A **164**, 291 (1997).

[20] J. Levy, V. Nikitin, J. M. Kikkawa, D. D. Awschalom, and N. Samarth, J. Appl. Phys. **79**, 6095 (1996).

[21] Y. Toda, S. Shinomori, K. Suzuki, and Y. Arakawa, Phys. Rev. B **58**, R10147 (1998).

[22] A. M. Mintairov, T. H. Kosel, J. L. Merz, P. A. Blagnov, A. S. Vlasov, V. M. Ustinov, and R. E. Cook, Phys. Rev. Lett. **87**, 277401 (2001).

[23] M. Ono, K. Matsuda, T. Saiki, K. Nishi, T. Mukaiyama, and M. Kuwata-Gonokami, Jpn. J. Appl. Phys., Part 2 **38**, L1460 (1999).

[24] T. Guenther, V. Emiliani, F. Intonti, C. Lienau, T. Elsaesser, R. Notzel, and K. H. Ploog, Appl. Phys. Lett. **75**, 3500 (1999).

[25] Y. Toda, T. Sugimoto, M. Nishioka, and Y. Arakawa, Appl. Phys. Lett. **76**, 3887 (2000).

[26] A. Chavez-Pirson, J. Temmyo, H. Kamada, H. Gotoh, and H. Ando, Appl. Phys. Lett. **72**, 3494 (1998).

[27] Y. Toda, S. Shinomori, K. Suzuki, and A. Arakawa, Appl. Phys. Lett. **73**, 517 (1998).

[28] D. Pahlke, F. Poser, E. Steimetz, M. Pristovsek, N. Esser, and W. Richter, Phys. Status Solidi A **170**, 401 (1998).

[29] I. Manke, J. Lorbacher, J. L. Spithoven, F. Heinrichsdorff, and M. Dahne-Preitsch, Surf. Interface Anal. **27**, 491 (1999).

[30] C. Obermuller, A. Deisenrieder, G. Abstreiter, K. Karrai, S. Grosse, S. Manus, J. Feldman, H. Lipsanen, M. Sopanen, and J. Ahopelto, Appl. Phys. Lett. **74**, 3200 (1999).

[31] H. D. Robinson and B. B. Goldberg, Phys. Rev. B **61**, R5086 (2000).

[32] T. Kawazoe, K. Kabayashi, J. Lim, Y. Narite, and M. Otsu, Phys. Rev. Lett. **88**, 067404 (2002).

[33] L. Jacak, P. Hawrylak, and A. Wojs, *Quantum Dots* (Springer, New York, 1998).

[34] D. Bimberg, M. Grundman, and N. N. Ledentsov, Quantum Dot Heterostructures (Wiley, Chichester, 1999).

[35] G. Chen, N. H. Bonadeo, D. G. Steel, D. Gammon, D. S. Katzer, D. Park, and L. J. Sham, Science **289**, 1906 (2000).

[36] F. Troiani, U. Hohenester, and E. Molinari, Phys. Rev. B **62**, R2263 (2000).

[37] P. Chen, C. Piermarocchi, and L. J. Sham, Phys. Rev. Lett. **87**, 067401 (2001).

[38] T. Guenther, V. Emiliani, F. Intoni, C. Lienau, T. Elsaesser, R. Notzel, and K. H. Ploog, Appl. Phys. Lett. **75**, 3500 (1999).

[39] G. Ortner, M. Bayer, A. Larionov, V. B. Timofeev, A. Forchel, Y.

B. Lyanda-Geller, T. L. Reinecke, P. Hawrylak, S. Fafard, and Z. Wasilewski, Phys. Rev. Lett. **90**, 086404 (2003).

[40] K. Matsuda, T. Matsumoto, H. Saito, K. Nishi, and T. Saiki, Physica E (Amsterdam) **7**, 377 (2000).

[41] Y. Toda, O. Moriwaki, M. Nishioka, and Y. Arakawa, Phys. Rev. Lett. **82**, 4114 (1999).

[42] A. C. Fischer-Cripps, *Nanointentation*, Mechanical Engineering Series (Springer-Verlag, New York, 2002).

[43] M. Cardona, in *Optical Properties and Band Structure of Germanium and Zinc Blende-Type Semiconductors*, in Proceedings of the International School of Physics ''Enrico Fermi,'' edited by E. Burstein (Academic, New York, 1972).

[44] D. E. Aspens, in *Handbook on Semiconductors*, edited by T. S. Moss (North–Holland, Amsterdam, 1980).

[45] A. A. Kaplyanskii, Opt. Spectrosc. **16**, 329 (1964).

[46] H. D. Robinson, M. G. Miller, B. B. Goldberg, and J. L. Merz, Appl. Phys. Lett. **72**, 2081 (1998).

[47] C. Obermuller, A. Deisenrieder, G. Abstreiter, K. Karrai, S. Grosse, S. Manus, J. Feldman, H. Lipsanen, M. Sopanen, and J. Ahopelto, Appl. Phys. Lett. **75**, 358 (1999).

[48] A. Chavez-Pirson, J. Temmyo, and H. Ando, Physica E (Amsterdam) **7**, 367 (2000).

[49] K. Ozasa and Y. Aoyagi, Physica E (Amsterdam) **13**, 212 (2002).

[50] P. B. Joyce, T. J. Krzyzewski, G. R. Bell, B. A. Joyce, and T. S. Jones, Phys. Rev. B **58**, R15981 (1998).

[51] D. Leonard, K. Pond, and P. M. Petroff, Phys. Rev. B **50**, 11687 (1994).

[52] K. H. Schmidt, G. Mederios-Ribeiro, U. Kunze, G. Abstreiter, M. Hagn, and P. M. Petroff, J. Appl. Phys. **84**, 4268 (1998).

[53] M. Grasii Alessi, M. Capizzi, A. S. Bhatti, A. Frova, F. Martelli, P. Frigeri, A. Bosacchi, and S. Franchi, Phys. Rev. B **59**, 7620 (1999).

[54] R. P. Mirin, K. L. Silverman, D. H. Christensen, and A. Roshko, J. Vac. Sci. Technol. B **18**, 1510 (2000).

[55] Qianghua Xie, J. L. Brown, and J. E. Van Nostrand, Appl. Phys. Lett. **78**, 2491 (2001).

[56] S. Anders, C. S. Kim, B. Klein, Mark W. Keller, R. P. Mirin, and A. G. Norman, Phys. Rev. B **66**, 125309 (2002).

[57] Landolt–Bernstein, *Numerical Data and Functional Relationships in Science and Technology*, New Series (Springer, Berlin, 1982), Vol. III/17a.

[58] I. Drauka and A.-L. Barabashi, Appl. Phys. Lett. **72**, 2102 (1998).

[59] V. A. Shchukin and D. Bimberg, Rev. Mod. Phys. **71**, 1125 (1999).

[60] A. Harootunian, E. Betzig, M. Isaacson, and A. Lewis, Appl. Phys. Lett. **49**, 674 (1986).

[61] J. A. Veeman, A. M. Otter, L. Kuipers, and N. F. van Hulst, Appl. Phys. Lett. **72**, 3115 (1998).

[62] G. E. Pikus and G. L. Bir *Symmetry and Strain Induced Effects in Semiconductors* (Wiley, New York, 1974).

[63] H. Hasegawa, Phys. Rev. **129**, 1029 (1963).

[64] F. H. Pollak and M. Cardona, Phys. Rev. **172**, 816 (1968).

[65] C. Priester, G. Allan, and M. Lannoo, Phys. Rev. B **37**, 8519 (1988).

[66] E. L. Ivchenko and G. E. Pikus, *Superlattices and Other Heterostructures. Symmetry and Optical Phenomena* (Springer, Berlin, 1997).

[67] S. P. Timoshenko and J. N. Goodier, *Theory of Elasticity* (McGraw–Hill, New York, 1970).

[68] A. M. Mintairov, P. A. Blagnov, O. V. Kovalenkov, C. Li, J. L. Merz, S. Oktyabrsky, V. Tokranov, A. S. Vlasov, and D. A. Vinokurov, Mater. Res. Soc. Symp. Proc. **722**, K11 (2002)2).

[69] G. Patriadche and E. Le Bourhis, Philos. Mag. A **82**, 1953 (2002).

[70] Le Bourhis and G. Patriadche, Phys. Status Solidi A **179**, 153 (2000).

[71] A. M. Mintairov, P. A. Blagnov, T. Kosel, J. L. Merz, V. M. Ustinov, A. S. Vlasov, and R. E. Cook, in Progress in Semiconductor Materials for Optoelectronic Applications, Materials Research Symposium Proceedings, 2002, Vol. 692, p. 85.

[72] I. E. Itskevich, M. Henini, H. A. Carmona, L. Eaves, P. C. Main, D. K. Maude, and J. C. Portal, Appl. Phys. Lett. **70**, 505 (1997).

[73] I. E. Itskevich, S. G. Lyapin, I. A. Troyan, P. C. Klipstein, L. Eaves, P. C. Main, and M. Henini, Phys. Rev. B **58**, R4250 (1998).

[74] J. Phillips, P. Bhattacharya, and U. Venkateswaran, Appl. Phys. Lett. **74**, 1549 (1999).

[75] K. Matsuda, T. Saiki, S. Nomura, M. Mihara, and Y. Aoyagi, Appl. Phys. Lett. **81**, 2291 (2002).

[76] R. Kotlyar, T. L. Reinecke, M. Bayer, and A. Forchel, Phys. Rev. B **63**, 085310 (2001).

[77] M. Bayer, S. N. Walck, T. L. Reinecke, and A. Forchel, Phys. Rev. B **57**, 6584 (1998).

[78] P. P. Paskov, P. O. Holtz, B. Monemar, J. M. Garcia, W. V. Schoenfeld, and P. M. Petroff, Phys. Rev. B **62**, 7344 (2000).

[79] A. Polimeni, S. T. Stoddart, M. Henini, L. Eaves, P. C. Main, K. Uchida, R. K. Hayden, and N. Miura, Physica E (Amsterdam) **2**, 662 (1998).

[80] O. Stier, M. Grundmann, and D. Bimberg, Phys. Rev. B **59**, 5688 (1999).

[81] *Properties of Lattice-Matched and Strained Indium Gallium Arsenide*, edited by P. Bhattacharya (INSPEC, London, 1993).

[82] J. Shumway, A. J. Williamson, A. Zunger, A. Passaseo, M. DeGiorgi, R. Chingolani, M. Catalano, and P. Crozier, Phys. Rev. B **64**, 125302 (2001).

[83] U. Woggon, W. Langbein, J. M. Hvam, A. Rosenauer, T. Remmele, and D. Gerthsen, Appl. Phys. Lett. **71**, 377 (1997).

[84] A. Rosenauer, U. Fischer, D. Gerthsen, and A. Foster, Appl. Phys. Lett. **71**, 3868 (1997).

[85] D. Hessman, P. Castrillo, M.-E. Pistol, C. Pryor, and L. Samuelson, Appl. Phys. Lett. **69**, 749 (1996).

[86] P. G. Blome, M. Wenderoth, M. Hubner, R. G. Ulbrich, J. Porsche, and F. Scholz, Phys. Rev. B **61**, 8382 (2000).

[87] C. Pryor, M.-E. Pistol, and L. Samuelson, Phys. Rev. B **56**, 10404 (1997).